A continuum damage analysis of hydrogen attack in a 2.25Cr–1Mo pressure vessel

Burg, M.W.D. van der; Giessen, E. van der; Tvergaard, V.

Published in:
Materials Science and Engineering A

DOI:
10.1016/S0921-5093(97)00466-8

Publication date:
1998

ELSEVIER

Materials Science and Engineering A241 (1998) 1–13

MATERIALS SCIENCE & ENGINEERING A

A continuum damage analysis of hydrogen attack in a 2.25Cr–1Mo pressure vessel

M.W.D. van der Burg [a], E. van der Giessen [a,*], V. Tvergaard [b]

[a] *Laboratory for Engineering Mechanics, Delft University of Technology, 2600 Delft, The Netherlands*
[b] *Department of Solid Mechanics, Technical University of Denmark, Lyngby, Denmark*

Received 10 February 1997; received in revised form 20 May 1997

Abstract

A micromechanically based continuum damage model is presented to analyze the stress, temperature and hydrogen pressure dependent material degradation process termed hydrogen attack, inside a pressure vessel. Hydrogen attack (HA) is the damage process of grain boundary facets due to a chemical reaction of carbides with hydrogen, thus forming cavities with high pressure methane gas. Driven by the methane gas pressure, the cavities grow, while remote tensile stresses can significantly enhance the cavitation rate. The damage model gives the strain-rate and damage rate as a function of the temperature, hydrogen pressure and applied stresses. The model is applied to study HA in a vessel wall, where nonuniform distributions of hydrogen pressure, temperature and stresses result in a nonuniform damage distribution over the vessel wall. Stresses inside the vessel wall first tend to accelerate and later decelerate the cavitation rate significantly. Numerical studies for different material parameters and different stress conditions demonstrate the HA process inside a vessel in time. Also, the lifetime of the pressure vessel is determined. The analyses underline that the general applicability of the Nelson curve is questionable. © 1998 Elsevier Science S.A.

Keywords: Hydrogen attack; Cavitation; Creep; Damage; Pressure vessel

1. Introduction

The operating conditions for many pressure vessels in the (petro)chemical industry are restricted by safety requirements to avoid hydrogen attack (HA) as one of the potential factors controlling their lifetime [1]. At the elevated temperatures and hydrogen pressures, hydrogen diffuses into the steel where it reacts with the carbides to form methane gas. The methane cannot diffuse away so that a cavity originates at the carbide location. The internal methane gas pressure drives further cavity growth. On grain boundaries, cavitation is relatively rapid due to the fast grain boundary diffusion. When cavity coalescence takes place at some facet, an intergranular microcrack is formed and when the microcracks link-up, macroscopic fracture ensues.

The cavitation can be accelerated by remotely applied tensile stress (e.g. the hoop stress in a vessel). While the damage is uniformly distributed along grain boundary facets in the absence of applied stresses, the presence of applied stresses tends to concentrate cavitation on facets perpendicular to the maximum principal stress. In most common operating conditions for vessels, the hydrogen pressure and/or the temperature decrease in the outward direction, so that the cavity gas pressure varies along the vessel radius. Also the stress distribution in the vessel wall may vary along the radius. This implies that the amount of HA damage is distributed nonuniformly over the vessel wall.

Even though such considerations suggest that HA in a component like a vessel may be a rather complex phenomenon in time and space, the design of C, Mo and Cr–Mo pressure vessel is generally based solely on so-called Nelson curves [1]. These empirical curves define for individual steels the regime in temperature vs hydrogen pressure space where operation is supposed to be safe. The attractiveness of the Nelson curves—their simplicity and generality—is at the same time an important weakness. The regime is presumed to be safe irrespective of the remote stress state and the heat treatment of the material which is known to be an important factor in the susceptibility to HA. Further-

* Corresponding author.

PII S0921-5093(97)00466-8

more, Nelson curves are of limited use when new steels, such as Modified 2.25Cr–1Mo, 2.25Cr–1Mo–V or 3Cr–1Mo–V, are introduced. A better understanding of HA and more sophisticated models or assessment techniques are therefore needed for this purpose.

Initial investigations on HA (see e.g. [2–6]) focused on the description of the evolution of a representative grain boundary cavity. The lifetime predictions were based on a single temperature and hydrogen pressure combination, and possible applied stresses were taken to remain constant during HA. In order to obtain a safe lifetime prediction, the most aggressive carbide was taken to determine the cavity pressure. If the stress state is estimated accurately, then the lifetimes obtained from these analyses (e.g. [3,4,6]) can be considered as first conservative predictions.

To improve the accuracy of such analyses, the interaction of the cavitation with adjacent grains was investigated [7]. As is well-known for intergranular creep cavitation, the cavity evolution can be significantly influenced by creep deformations of the surrounding grains [8–10]. Also HA cavitation due to nonuniform distributions of carbides along the grain boundaries in a polycrystal aggregate was analyzed numerically. It was found [7] that internal stresses developed to constrain the cavitation evolution around the most aggressive carbides significantly, thus increasing the lifetime. However, in these analyses the temperature and hydrogen pressure were still assumed constant, which may be questionable in industrial components under operating conditions. In order to enable the analysis of HA in such components, a damage model was derived in [11], which captured the numerical polycrystal HA results sufficiently well. This damage model is based on the description of two extreme cavitation modes. In one extreme, creep deformations of the grains are negligible, thus leading to uniform cavitation along all grain boundary facets and a hydrostatic dilation of the polycrystal aggregate. This mode is the so-called 'rigid grain mode'. In the opposite mode, creep deformations are significant and most cavitation is on facets oriented perpendicular to the maximum macroscopic principal stress. For this mode, Tvergaard's [12] damage model for creep failure by grain boundary cavitation was adopted and modified for HA.

In this paper, the damage model is used to numerically study the HA evolution in a 2.25Cr–1Mo pressure vessel (sketched in Fig. 1), taking into account variations in temperature from the inside T_i to the outside, T_o and variations in hydrogen pressure p_{H_2}. Due account is also given of possible stress redistributions during the HA cavitation. The approach is similar to Tvergaard's analysis of creep cavitation in furnace tubes [12]. The sensitivity of the HA evolution on aspects like carbide stability or on increase of temperature and hydrogen pressure is investigated. A few explorative results have been reported in [13].

The formulation of the theory is carried out in tensor notation, with tensors being denoted by bold face characters. The scalar or double-dot product between two second order tensors $\boldsymbol{A}$ and $\boldsymbol{B}$ is denoted as $\boldsymbol{A}:\boldsymbol{B}$, so that $\boldsymbol{A}:\boldsymbol{B} = A^{ij}B_{ij}$ with A^{ij} and B_{ij} being their contravariant and covariant components, respectively. The tensor product is denoted by $\otimes$ and the inner product by a single dot. The unit tensor is denoted by $\boldsymbol{I}$. Tensors $\boldsymbol{m}_1$, $\boldsymbol{m}_2$ and $\boldsymbol{m}_3$ are defined through $\boldsymbol{m}_i = \boldsymbol{n}_i \otimes \boldsymbol{n}_i$ (no summation on $i = 1, \ldots, 3$) in terms of orthonormal vectors $\boldsymbol{n}_i$. In this paper, the $\boldsymbol{n}_i$ coincide with cylindrical coordinate directions: $\boldsymbol{n}_1$ is axial, $\boldsymbol{n}_2$ is radial and $\boldsymbol{n}_3$ is circumferential, as displayed in Fig. 1.

2. Relations concerning cavitation

At operating conditions for the pressure vessel, the hydrogen dissociates into atoms and diffuses through the steel due to the hydrogen pressure gradient over the vessel wall. Inside the steel, some hydrogen atoms associate again to form hydrogen molecules at discontinuities like grain boundaries or carbides. This hydrogen gas can react with the carbides present in the steel. The equilibrium reaction can be written in generalized form as:

$$M_xC_y + 2yH_2 \rightleftarrows yCH_4 + xM \tag{1}$$

with x the number of metal atoms (M) and y the number of carbon atoms (C) in the carbide. The methane molecules are much larger than the hydrogen atoms and cannot diffuse through the steel. The equilibrium methane pressure inside the cavity thus formed, p_{CH_4}, depends on the stability of the carbide. The internal cavity pressure p_m is due to a mixture of the methane gas and hydrogen, with partial pressures p_{CH_4} and p_{H_2}, respectively. The total pressure in this non-ideal gas mixture p_m is approximately given by:

$$p_m = p_{CH_4} + p_{H_2}. \tag{2}$$

Driven by this internal pressure p_m, the cavity expands, as will be discussed later. Nevertheless, it is assumed here that the equilibrium methane pressure is reached

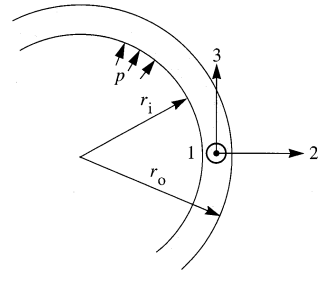

Fig. 1. Part of cross section of the pressure vessel, with coordinate system used.

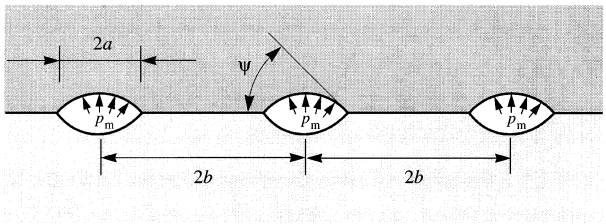

Fig. 2. Spherical-cap shaped cavities on a grain boundary facet with tip angle ψ. The radius of the cavity is a, the spacing between the cavities is $2b$.

during growth in all situations. By incorporating the reaction kinetics into their model for cavity growth, Shih and Johnson [2] showed however that the equilibrium pressure is not reached in certain cases. Hence, our assumption of constant pressure implies that the cavitation rate is overestimated. We have chosen here not to incorporate the reaction kinetics into our model, in view of other, related assumptions that are being made, such as the assumption that the carbides are present from the beginning and that the nucleation time of cavities is negligible compared to the lifetime. Also, the methane pressure is considered to be completely determined by the reaction of hydrogen with the carbide, thus neglecting the supply of carbon from the grains to the grain boundary. Finally, we assume that the rate of supply of hydrogen is so fast compared to the time scale of the HA damage process that sufficient hydrogen is available at all times.

A cavity is modelled as a hole with spherical-cap shaped surfaces, which can be characterized by its radius a and tip angle ψ (see Fig. 2). The average spacing between cavities is $2b$. The volume of a cavity V is given by $V=\frac{4}{3}\pi a^3 h(\psi)$, where the geometric parameter $h(\psi)$ is defined as $h(\psi)=[(1+\cos\psi)^{-1}-\frac{1}{2}\cos\psi]/\sin\psi$.

At the elevated temperatures, the pressurized cavities grow by grain boundary diffusion in combination with Norton power law creep in the adjacent grains. In accordance with the diffusion and creep process, the cavity growth rate $\dot{V}$ can be split up into a part based on diffusive cavity growth, $\dot{V}_{\text{diff}}$ and a part due to dislocation creep, $\dot{V}_{\text{cr}}$. The total volumetric growth rate is $\dot{V}=\dot{V}_{\text{diff}}+\dot{V}_{\text{cr}}$. The gas pressure p_{m} is the direct driving force for cavity growth, but the stress state remote from the cavity, denoted by $\boldsymbol{\sigma}$, can significantly affect the growth rate. Tensile stress will accelerate evolution, whereas compressive stress will have the opposite effect, as can be seen directly in the forthcoming growth relations. The remote stress state $\boldsymbol{\sigma}$ enters into the cavity growth relations through the facet normal stress σ_{n}, the Von Mises effective stress σ_{e} and the mean stress σ_{m}, all remote from the cavity.

Box 1

$\boldsymbol{s}$	stress deviator	$\boldsymbol{n}$	normal on facet
$\dot{\varepsilon}_{\text{T}}$	reference strain-rate parameter	$\mathcal{D}$	grain boundary diffusion parameter
σ_0	reference stress parameter	sign	sign of its argument
n	creep exponent		

$$\sigma_{\text{n}}=\boldsymbol{n}\cdot\boldsymbol{\sigma}\cdot\boldsymbol{n} \qquad \sigma_{\text{m}}=(\sigma:\boldsymbol{I})/3 \qquad \sigma_{\text{e}}=\sqrt{\tfrac{3}{2}\boldsymbol{s}:\boldsymbol{s}} \qquad \boldsymbol{s}=\boldsymbol{\sigma}-\sigma_{\text{m}}\boldsymbol{I} \qquad \dot{\varepsilon}_{\text{e}}^{\text{c}}=\dot{\varepsilon}_{\text{T}}\left(\frac{\sigma_{\text{e}}}{\sigma_0}\right)^n$$

$$\dot{\varepsilon}_{\text{m}}=\dot{\varepsilon}_{\text{T}}\left|\frac{\sigma_{\text{m}}+p_{\text{m}}}{\sigma_0}\right|^n \qquad \alpha_n=3/(2n) \qquad \beta_n=(n-1)\,(n+0.4319)/n^2$$

$$\dot{V}_{\text{cr}}^{\text{L}}=2\pi\dot{\varepsilon}_{\text{m}}a^3h(\psi)\,\text{sign}(\sigma_{\text{m}}+p_{\text{m}})\,r$$

$$\text{where}\quad \begin{cases} r=\left[\alpha_n+\beta_n\left|\dfrac{\sigma_{\text{e}}}{\sigma_{\text{m}}+p_{\text{m}}}\right|\right]^n & \text{if } \left|(\sigma_{\text{m}}+p_{\text{m}})/\sigma_{\text{e}}\right|\geq 1 \\ r=[\alpha_n+\beta_n]^n\left|\dfrac{\sigma_{\text{e}}}{\sigma_{\text{m}}+p_{\text{m}}}\right|^{n-1} & \text{if } \left|(\sigma_{\text{m}}+p_{\text{m}})/\sigma_{\text{e}}\right|<1 \end{cases}$$

$$\dot{V}_{\text{diff}}^{\text{L}}=4\pi\mathcal{D}\frac{\sigma_{\text{n}}+p_{\text{m}}}{\ln(1/f)-\frac{1}{2}(3-f)\,(1-f)}$$

$$f=\max\left[\left(\frac{a}{b}\right)^2,\left(\frac{a}{a+1.5L}\right)^2\right] \qquad L=\left(\mathcal{D}\sigma_{\text{e}}/\dot{\varepsilon}_{\text{e}}^{\text{c}}\right)^{1/3}$$

$$\dot{V}_{\text{cr}}^{\text{H}}=2\pi\dot{\varepsilon}_{\text{m}}a^3h(\psi)\text{sign}(\sigma_{\text{m}}+p_{\text{m}})\left[\frac{1}{1-(0.87a/b)^{3/n}}\right]^n s$$

$$\text{where}\quad \begin{cases} s=\left(\alpha_n+\dfrac{1}{n}\dfrac{\text{sign}(\sigma_{\text{n}}-\sigma_{\text{m}})}{\text{sign}(\sigma_{\text{m}}+p_{\text{m}})}\left|\dfrac{\sigma_{\text{e}}}{\sigma_{\text{m}}+p_{\text{m}}}\right|\right)^n & \text{if } \left|(\sigma_{\text{m}}+p_{\text{m}})/\sigma_{\text{e}}\right|\geq 1 \\ s=\left(\alpha_n+\dfrac{1}{n}\dfrac{\text{sign}(\sigma_{\text{n}}-\sigma_{\text{m}})}{\text{sign}(\sigma_{\text{m}}+p_{\text{m}})}\right)\left|\dfrac{\sigma_{\text{e}}}{\sigma_{\text{m}}+p_{\text{m}}}\right|^{n-1} & \text{if } \left|(\sigma_{\text{m}}+p_{\text{m}})/\sigma_{\text{e}}\right|<1 \end{cases}$$

$$\dot{V}_{\text{diff}}^{\text{H}}=4\pi\mathcal{D}\frac{\sigma_{\text{n}}+p_{\text{m}}}{\ln(1/f)-\frac{1}{2}(3-f)\,(1-f)} \qquad f=\left(\frac{a}{b}\right)^2$$

$$\dot{V}=\max\left[\dot{V}_{\text{cr}}^{\text{L}}+\dot{V}_{\text{diff}}^{\text{L}},\dot{V}_{\text{cr}}^{\text{H}}+\dot{V}_{\text{diff}}^{\text{H}}\right]$$

contains a summary of the cavity growth relations; the relations are described in detail in [6] and build on work in e.g. [12,14–17]. Sintering stresses are neglected in the analyses since they do not affect time to failure [6]. It is noted that the growth relations involve two modes of creep cavity growth, indicated by H and L in Box 1, as established in [5]. (Roughly speaking, the relations indicated by L are relevant at low stress triaxialities and small damage levels; the relations labeled H operate at high stress triaxialities and larger damage levels). Due to the coupling between diffusive growth and creep growth, the diffusive growth rate in general depends on this mode; but, in case of negligible creep deformations around the cavities, $\dot{V}_{\text{diff}}^{\text{L}}=\dot{V}_{\text{diff}}^{\text{H}}$.

The temperature dependence of the diffusion and creep parameters in the growth relations is taken according to a standard Arrhenius law and is expressed as:

$$\mathcal{D}=\mathcal{D}_0\frac{T_0}{T}\exp\left[\frac{Q_{\text{B}}}{R}\left(\frac{1}{T_0}-\frac{1}{T}\right)\right],$$

$$\dot{\varepsilon}_T=\dot{\varepsilon}_0\frac{T_0}{T}\exp\left[\frac{Q_{\text{V}}}{R}\left(\frac{1}{T_0}-\frac{1}{T}\right)\right], \tag{3}$$

where T_0 is a reference temperature, $\dot{\varepsilon}_0$ and $\mathscr{D}_0$ the reference creep rate and diffusion coefficients at T_0, Q_V and Q_B are activation energies and R is the gas constant. Following Needleman and Rice [15] and Frost and Ashby [18], the reference creep strain-rate parameter $\dot{\varepsilon}_0$ and the boundary diffusion parameter $\mathscr{D}_0$ are taken to be given by:

$$\dot{\varepsilon}_0 = A\frac{D_{V0}\mu b}{kT_0}\left(\frac{\sigma_0}{\mu}\right)^n \exp\left[\frac{-Q_V}{RT_0}\right],$$
$$\mathscr{D}_0 = \frac{D_{B0}\delta_B\Omega}{kT_0}\exp\left[\frac{-Q_B}{RT_0}\right], \quad (4)$$

where A is a creep constant, subscript V refers to volume (or lattice) diffusion, subscript B refers to boundary diffusion, μ is the elastic shear modulus, b is the length of the Burger's vector, k is the Boltzmann's constant, δ_B is the thickness of the boundary and Ω is the atomic volume.

During cavity growth, the spherical-cap shape of the cavity is assumed to be maintained by rapid surface diffusion throughout the process, according to observations for 2.25Cr–1Mo steels in [19]. Then, from the volumetric rate of change $\dot{V}$, the growth rate of the cavity radius is found as:

$$\dot{a} = \dot{V}/(4\pi a^2 h(\psi)). \quad (5)$$

In the model, the cavities would coalesce with neighbouring cavities when $a/b = 1$ (see Fig. 2). However, it is observed for intergranular creep rupture that failure of the grain boundary occurs before actual coalescence, e.g. due to tearing of the ligament [20]. Since HA cavitation is micromechanically analogous to creep rupture, we assume that also in this case ligament failure takes place earlier; we assume cavity coalescence when $a/b = 0.7$.

In view of the application of the cavity growth relations in a damage model to be discussed presently, it is important to realize that these relations are based on considerations of axisymmetric states of stress [5], [15–17]. Like in previous applications (e.g. [12]), it will be assumed that these expressions still give a reasonable estimate under arbitrary 3-D stress states through the corresponding mean stress and effective stress.

3. Damage model

The damage model for HA is based on a representative volume element (RVE) of the polycrystalline metal consisting of many grains and where the carbides are identical and distributed uniformly along the grain boundaries. The damage model gives the strain-rate and damage rate as a function of the stress $\boldsymbol{\Sigma}$ that the RVE is subjected to. Such quantities referring to the RVE are termed macroscopic and are represented with upper-case characters. Lower-case variables represent parameters at the size scale of grain boundaries, as in the previous section. The initial formulation of the damage model for HA was given in [11]; the presentation here will introduce a small extension.

The total macroscopic strain-rate is split in the elastic strain-rate $\boldsymbol{D}^E$, the thermal strain-rate $\boldsymbol{D}^T$ and the inelastic strain-rate $\boldsymbol{D}^{CC}$ due to creep and cavitation; thus, $\boldsymbol{D} = \boldsymbol{D}^E + \boldsymbol{D}^T + \boldsymbol{D}^{CC}$. The elastic response of the RVE is taken to follow Hooke's law and it is assumed that the HA cavitation does not significantly affect the elastic behaviour. The elastic stress-strain relation is written here on the rate form $\overset{\triangledown}{\boldsymbol{\Sigma}} = \mathscr{R}:\boldsymbol{D}^E$, where $\overset{\triangledown}{\boldsymbol{\Sigma}}$ is the Jaumann stress rate and $\mathscr{R}$ is the fourth order tensor of elastic moduli. Elimination of the elastic strain-rate yields

$$\overset{\triangledown}{\boldsymbol{\Sigma}} = \mathscr{R}:(\boldsymbol{D} - \boldsymbol{D}^T - \boldsymbol{D}^{CC}). \quad (6)$$

For an isotropic material, the dilation-rate due to thermal expansion is given by:

$$\boldsymbol{D}^T = \alpha\dot{T}\boldsymbol{I}, \quad (7)$$

where α is the linear thermal expansion coefficient and $\dot{T}$ is the rate of change of the absolute temperature. If there were no cavitation, $\boldsymbol{D}^{CC}$ would be simply equal to the power law creep rate $\boldsymbol{D}^C$ defined by:

$$\boldsymbol{D}^C = \dot{E}^c_e\frac{3}{2}\frac{\boldsymbol{S}}{\Sigma_e}, \quad (8)$$

where $\dot{E}^c_e = \dot{\varepsilon}_T(\Sigma_e/\sigma_0)^n$ is the macroscopic effective creep rate of the undamaged material (i.e. defined like $\dot{\varepsilon}^c_e$ but in terms of the macroscopic effective stress Σ_e).

As explained in detail in [11], the creep-cavitation strain-rate $\boldsymbol{D}^{CC}$ is determined by one of two possible cavitation modes. In the one mode, the cavitation damage is virtually uniform along all facets. In the second mode, cavitation predominantly takes place on the facets perpendicular to the maximum principal stress component of the macroscopic stress $\boldsymbol{\Sigma}$. The mode yielding the highest cavitation rate is taken to be the active mode.

A convenient parameter to indicate which mode is active is $\dot{\delta}/(R_I\dot{E}^c_e)$, where R_I is the average initial grain boundary facet radius and $\dot{\delta}$ denotes the cavitation rate. The latter is determined through the separation δ of adjacent grains due to grain boundary cavitation, which is defined as $\delta = V/(\pi b^2)$. Differentiation with respect to time gives the separation rate,

$$\dot{\delta} = \frac{\dot{V}}{\pi b^2} + \delta\boldsymbol{n}\cdot\boldsymbol{d}^c\cdot\boldsymbol{n}, \quad (9)$$

where $\boldsymbol{d}^c = (3/2)\,\dot{\varepsilon}^c_e\,\boldsymbol{s}/\sigma_e$ and $\boldsymbol{n}$ is the facet normal vector. The second term in the right-hand side of Eq. (9) reflects the rate of change of the cavity spacing $\dot{b}$ due to creep in the plane of the grain boundary facets, which can be written as $\dot{b}/b = -\boldsymbol{n}\cdot\boldsymbol{d}^c\cdot\boldsymbol{n}/2$ by virtue of $\boldsymbol{I}:\boldsymbol{d}^c = 0$ (under typical operating conditions, this contribution to $\dot{\delta}$ is very often negligible). So, the value of the parameter $\dot{\delta}/(R_I\dot{E}^c_e)$

depends on the ratio of the creep deformations of the grains and the cavitation rate along the grain boundaries.

When creep deformations of the grains are significant, i.e. $\dot{\delta}/(R_I\dot{E}^c_e)$ is small, grain boundary cavitation can be described in terms of a penny shaped crack model. In this model, the cavitation on grain boundary facets is determined by matching the crack opening rate of a virtual penny shaped crack with the cavitation rate on the grain boundary. Such a model has been adopted for intergranular creep failure by Tvergaard [9,12], based on an idea of Rice [21]. In most applications [9,12] of the penny shaped crack model, the macroscopic stress state was close to uniaxial and the maximum principal stress retained more or less the same direction. Then, most cavitated facets are oriented perpendicular to the maximum macroscopic principal stress direction and therefore only these facets were taken into account in the damage model. However here, in the presence of HA, it is possible that the maximum principal stress direction will change during lifetime, or that the stress states are more biaxial or even hydrostatic. Therefore, we here extend the penny shaped crack model by determining the cavitation rate in all three principal stress directions.

The crack opening rate of the virtual penny shaped crack perpendicular to the i-direction is given by

$$\dot{\delta}_{p,i}=\frac{4}{\pi}\left(1+\frac{3}{n}\right)^{-1/2}\frac{\boldsymbol{\Sigma}:\boldsymbol{m}_i-\sigma_{n,i}}{\Sigma_e}\dot{E}^c_e 2R_i \tag{10}$$

This expression was derived first by He and Hutchinson [22] and modified in [12] for the fact that the cavitating facet can still transmit a normal stress $\sigma_{n,i}$ rather than being stress free. The radius of the virtual crack (the cavitating facet) perpendicular to the i-direction is R_i. The magnitude of the normal stress $\sigma_{n,i}$ is determined by requiring at any instant that $\dot{\delta}_{p,i}(\sigma_{n,i})$ according to Eq. (10) is equal to the cavitation rate $\dot{\delta}(\sigma_{n,i})$ determined from Eq. (9) and the cavity growth relations in Box 1 for a facet normal stress $\sigma_{n,i}$. The effective stress $\sigma_{e,i}$ and mean stress $\sigma_{m,i}$ at the grain boundary facet, also needed to determine the cavitation rate $\dot{\delta}(\sigma_{n,i})$, are determined from the creep strain-rates in the plane of the facet. The latter are equal to the grain creep strain-rates to ensure compatibility between the facet cavitation and the polycrystal deformations; hence, $\sigma_{e,i}=\Sigma_e$. For the mean stress we then find [11] $\sigma_{m,i}=\sigma_{n,i}-\boldsymbol{S}:\boldsymbol{m}_i$, where $\boldsymbol{S}$ is the macroscopic stress deviator.

The RVE strain-rate in this penny shaped crack model is given by:

$$\boldsymbol{D}^{CC}_p=\dot{E}^c_e\left[\frac{3}{2}\frac{\boldsymbol{S}}{\Sigma_e}\left(1+\rho\sum_{k=1}^{3}\left(\frac{n-1}{n+1}\right)\left(\frac{\boldsymbol{\Sigma}:\boldsymbol{m}_k-\sigma_{n,k}}{\Sigma_e}\right)^2\right)+\rho\sum_{k=1}^{3}\boldsymbol{m}_k\left(\frac{2}{n+1}\frac{\boldsymbol{\Sigma}:\boldsymbol{m}_k-\sigma_{n,k}}{\Sigma_e}\right)\right]. \tag{11}$$

This expression is based on [23] and [12] and in particular follows the suggestion in [12] to account for the contribution of multiple families of cavitating facets. The parameter in Eq. (11) depends on the number of cavitating facets per unit volume, N, and the initial radius of the penny shape crack, R_I, and is defined by $\rho=4R_I^3N(n+1)/\sqrt{(1+3/n)}$. Because all grain boundaries perpendicular to a principal stress direction can cavitate, the number of facets per unit volume N associated to any principal stress direction is $N=1/\bar{V}_{gr}$, with $\bar{V}_{gr}$ the average volume of a grain. Assuming regular truncated octahedrons, one finds $N=0.042\,R_I^{-3}$ where the radius R_I is based on the average facet surface of the truncated octahedron. It is noted that in the case of intergranular creep cavitation (no internal cavity pressure) and when the macroscopic stress state is uniaxial, the cavitation contribution of the non-maximum principal stress directions in Eq. (11) vanishes and the expression reduces to that in [12]. Also note that in the penny shaped crack model, the facets are assumed to be isolated even when cavitation takes place on facets normal to either one of the three directions. If interaction takes place between the cavitating facets, the rigid grain mode to be discussed presently, will become active [7].

If creep of the grains can be neglected relative to the grain boundary cavitation rate, i.e. when $\dot{\delta}/(R_I\dot{E}^c_e)$ is large, the so-called rigid grain model is active [7,11]. In this model, cavitation is uniform along all facets in the RVE (recall that the carbides are assumed to be identical and uniformly distributed over all facets). What is essential in this model is the coupling of the cavitation rates on different facets. Due to the relatively small creep strain-

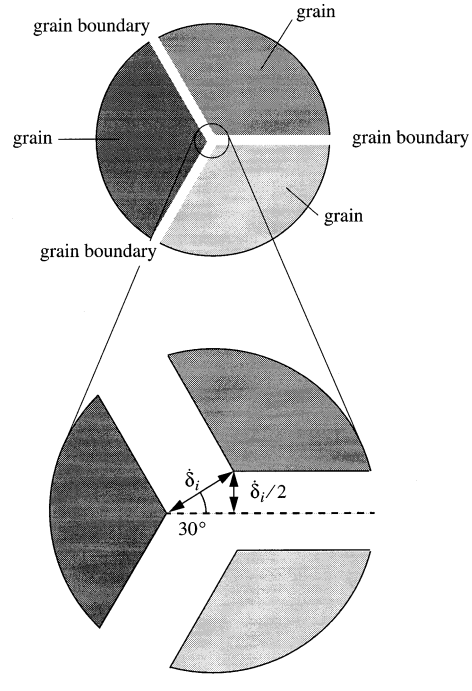

Fig. 3. Geometrical coupling of the cavitation rate on different facets in the rigid grain mode.

rates inside the grains, the grains behave as virtually rigid, resulting in a geometrical coupling of the cavitation rates $\dot{\delta}$ as is illustrated in Fig. 3. Because all facets cavitate in the rigid grain model, including those facets that are not perpendicular to the macroscopic maximum principal stress, the cavitation results in a macroscopic hydrostatic dilation of the RVE. The macroscopic strain-rate $\boldsymbol{D}^{\mathrm{CC}}_{\mathrm{rg}}$ thus consists of a pure (yet small) creep part and a dilational part due to the isotropic cavitation $\dot{\delta}_{\mathrm{rg}}$, i.e.

$$\boldsymbol{D}^{\mathrm{CC}}_{\mathrm{rg}} = \dot{E}^{\mathrm{c}}_{\mathrm{e}} \frac{3}{2} \frac{\boldsymbol{S}}{\Sigma_{\mathrm{e}}} + \kappa \frac{\dot{\delta}_{\mathrm{rg}}}{R_{\mathrm{I}}} \boldsymbol{I}. \tag{12}$$

Here, κ is a geometrical parameter for the dilation, which depends on the grain shape; $\kappa = 0.31$ for grains having the shape of truncated octahedrons [11]. The stress component that is conjugate to the hydrostatic dilation is the macroscopic mean stress $\Sigma_{\mathrm{m}} = (\boldsymbol{\Sigma}:\boldsymbol{I})/3$. Therefore, the normal stress governing the cavitation rate $\dot{\delta}_{\mathrm{rg}}$ $(\sigma_{\mathrm{n,rg}})$ is taken to be $\sigma_{\mathrm{n,rg}} = \Sigma_{\mathrm{m}}$. For the current value of the cavitation parameters a and b to be substituted into the cavity growth relations, the cavity half spacing b is taken as the average over the three directions and the cavity radius a is determined by the average separation $\bar{\delta}$, i.e. $a = [(3/4)\,\bar{\delta} b^2/h(\psi)]^{1/3}$.

Given these two extreme modes of cavitation, there are different ways to construct an approximate description of cavitation for all relevant states. Here, as in [13], we adopt an approach in which a straightforward criterion is used to determine which of the two deformation modes is active, namely the one which yields the (absolute) maximum cavitation rate $\dot{\delta}$ (properly accounting for the signs of the driving stresses), i.e.

$$\dot{\delta} = \max \left[\dot{\delta}_{\mathrm{p},i} \frac{\boldsymbol{\Sigma}:\boldsymbol{m}_i}{|\boldsymbol{\Sigma}:\boldsymbol{m}_i|}, \dot{\delta}_{\mathrm{rg}} \frac{\Sigma_{\mathrm{m}}}{|\Sigma_{\mathrm{m}}|} \right] \quad (i = 1, \ldots, 3) \text{ (no summation)}. \tag{13}$$

If the maximum cavitation rate is determined by the penny shaped crack model, the damage states in the three directions are updated independently with their local $\dot{a}_i$. If the rigid grain model delivers the highest cavitation rate, the cavitation on each facet is updated with the same separation rate $\dot{\delta}_{\mathrm{rg}}$, taking account of the local creep deformations $\delta \boldsymbol{n} \cdot \boldsymbol{d}^{\mathrm{c}} \cdot \boldsymbol{n}$. The radius R_i and the cavity half spacing b_i are updated according to the local facet creep strain-rates; i.e. the facet radius R_i changes according to $\dot{R}_i/R_i = -\boldsymbol{n} \cdot \boldsymbol{d}^{\mathrm{c}} \cdot \boldsymbol{n}/2$ and the ratio b_i/R_i remains constant. The maximum cavitation rate on the ith facet in the penny shaped crack model also determines the grain boundary mean stress in the rigid grain model by $\sigma_{\mathrm{m,rg}} = \sigma_{\mathrm{n,rg}} - \boldsymbol{S}:\boldsymbol{m}_i$, assuming that the creep strain-rates on that facet are most important.

Substitution of either one of the expressions Eq. (11) or Eq. (12) for $\boldsymbol{D}^{\mathrm{CC}}$, as decided by Eq. (13), along with Eq. (7) into Eq. (6) yields the final rate constitutive equation.

The complete damage state in the RVE can be characterized at each moment by a second-order damage tensor, $\boldsymbol{\varphi}$, which is defined here as:

$$\boldsymbol{\varphi} = \sum_{i=1}^{3} R_i^3 N_i (a/b)_i^2 \boldsymbol{m}_i^{\varphi}, \tag{14}$$

similar to definitions by Onat and Leckie [24] and by Murakami [25]. Here, $\boldsymbol{m}_i^{\varphi}$ $(i = 1, \ldots, 3)$ are the three principal damage tensor directions (defined similar to the $\boldsymbol{m}_i$) and N_i is the number of facets per unit volume normal to the ith principal direction (for the above mentioned regular truncated-octahedral grains $N_i = N$).

While following the material degradation process in the pressure vessel of Fig. 1, (the components of) the damage tensor changes continuously. However, not all parameters in the right-hand side of Eq. (14) contribute equally to the rate of change of $\boldsymbol{\varphi}$. First of all, the principal directions $\boldsymbol{m}_i^{\varphi}$ of the damage tensor and those of the stress tensor coincide and remain fixed throughout the process. Furthermore, as mentioned before, the initial number of cavitating facets N_i and the initial facet radius R_i are assumed to be distributed uniformly in our material microstructure. Since the strains in the pressure vessel remain small, as will be shown later, the changes of N_i and R_i are negligible. Hence, the only interesting contribution for the analysis of the vessel is the evolution of the porosity $(a/b)_i$.

4. Computational method

For the numerical applications of the damage model presented above we shall use a finite strain description, for which we adopt a scheme based on a Lagrangian formulation of the field equations. A finite strain formulation is adopted in order to account for rupture effects associated with geometry changes. Following [12], convected coordinates x^i are used, so that if $\boldsymbol{g}_i$ are the base vectors in the undeformed configuration corresponding to x^i, the deformed base vectors are $\boldsymbol{G}_i = \boldsymbol{F} \cdot \boldsymbol{g}_i$ ($\boldsymbol{F}$ is the deformation gradient tensor) with G_{ij} being the associated metric coefficients. Their determinant is denoted by G and in terms of the corresponding value g in the undeformed configuration, we have $\det(\boldsymbol{F}) = \sqrt{G/g}$. The initial, undeformed configuration of the body with volume V and surface S is used as a reference. Then, for quasi-static deformations, the equilibrium equations are expressed through the virtual work condition. In view of the type of the constitutive relation Eq. (6), a linear incremental solution procedure is used, which is based on the rate of virtual work condition:

$$\Delta t \int_V (\dot{\tau}^{ij}\,\delta\eta_{ij} + \tau^{ij}\,v^k_{j,i}\,\delta v_{k,j})\,\mathrm{d}V = \Delta t \int_S \dot{T}^i \delta\, v_i\,\mathrm{d}S - \left[\int_V \tau^{ij}\,\delta\eta_{ij}\,\mathrm{d}V - \int_S T^i\,\delta v_i\,\mathrm{d}S\right] \tag{15}$$

for arbitrary variations of the velocity components v_i and corresponding variations of the components of the Lagrangian strain-rate tensor $\dot{\boldsymbol{\eta}} = \boldsymbol{F}^T \cdot \boldsymbol{D} \cdot \boldsymbol{F}$. In Eq. (15), $\dot{\eta}_{ij}$ and τ^{ij} are the components on the undeformed basis of $\dot{\boldsymbol{\eta}}$ (or, equivalently, the components of the Eulerian strain-rate tensor $\boldsymbol{D}$ on the deformed basis) and of the second Piola-Kirchhoff tensor $\boldsymbol{\tau} = (\det\boldsymbol{F})\,\boldsymbol{F}^{-1}\cdot\boldsymbol{\Sigma}\cdot\boldsymbol{F}^{T-1}$ corresponding to $\boldsymbol{\Sigma}$ (or, equivalently, the components of the Kirchhoff tensor $(\det\boldsymbol{F})\boldsymbol{\Sigma}$ on the deformed basis); T^i are the corresponding traction vector components. The bracketed terms in Eq. (15) entail an equilibrium correction.

Implementation of the damage model in the condition Eq. (15) requires that Eqs. (6), (7), (11) and (12) be transformed into Lagrangian quantities τ^{ij} and $\dot{\eta}_{ij}$. This leads to:

$$\dot{\tau}^{ij} = \mathscr{L}^{ijkl}\,\dot{\eta}_{kl} - \sqrt{\frac{G}{g}}\,\{\dot{E}^{\mathrm{c}}_{\mathrm{e}}\,\mathscr{R}^{ijkl}\,N_{kl} + \dot{\Delta}^{ij}\}, \tag{16}$$

where

$$\mathscr{L}^{ijkl} = \sqrt{\frac{G}{g}}\,\mathscr{R}^{ijkl} - \frac{1}{2}(\tau^{ik}G^{jl} + \tau^{jk}G^{il} + \tau^{jl}G^{ik} + \tau^{il}G^{jk}) + \tau^{ij}G^{kl}, \tag{17}$$

and where N_{ij} and $\dot{\Delta}_{ij}$ depend on the cavitation mode, i.e.

- penny shaped crack mode (scriptum 'p'):

$$N_{ij} = (1/\dot{E}^{\mathrm{c}}_{\mathrm{e}})(\boldsymbol{G}_i \cdot \boldsymbol{D}^{\mathrm{CC}}_{\mathrm{p}} \cdot \boldsymbol{G}_j), \qquad \dot{\Delta}^{ij} = \mathscr{R}^{ijkl}\,G_{kl}\alpha\dot{T}; \tag{18}$$

- rigid grain mode (scriptum 'rg'):

$$N_{ij} = (1/\dot{E}^{\mathrm{c}}_{\mathrm{e}})(\boldsymbol{G}_i \cdot \boldsymbol{D}^{\mathrm{C}} \cdot \boldsymbol{G}_j),$$
$$\dot{\Delta}^{ij} = \mathscr{R}^{ijkl}\,G_{kl}\,(\alpha\dot{T} + \kappa\dot{\delta}_{\mathrm{rg}}/R_{\mathrm{I}}). \tag{19}$$

Note that the contribution to the creep-cavitation strain-rate $\boldsymbol{D}^{\mathrm{CC}}$ that is due to the cavitation damage is incorporated into N_{ij} for the penny shaped crack mode, while this contribution for the rigid grain mode is included in the dilational term $\dot{\Delta}_{ij}$.

For the time integration of the governing equations, we adopt a forward gradient method that is a direct extension of that used in [12] for the present constitutive equations. The method is based on recognizing the strong nonlinearity involved in the power law expression for the macroscopic creep rate $\dot{E}^{\mathrm{c}}_{\mathrm{e}}$. Therefore, the value of $\dot{E}^{\mathrm{c}}_{\mathrm{e}}$ to be substituted in Eq. (16) is expressed in terms of the values at time t and $t+\Delta t$ through:

$$\dot{E}^{\mathrm{c}}_{\mathrm{e}} = (1-\theta)\,\dot{E}^{\mathrm{c}_{(t)}}_{\mathrm{e}} + \theta\dot{E}^{\mathrm{c}_{(t+\Delta t)}}_{\mathrm{e}}, \tag{20}$$

where $\dot{E}^{\mathrm{c}_{(t+\Delta t)}}_{\mathrm{e}}$ is estimated through the Taylor expansion:

$$\dot{E}^{\mathrm{c}_{(t+\Delta t)}}_{\mathrm{e}} = \dot{E}^{\mathrm{c}_{(t)}}_{\mathrm{e}} + \frac{\partial\dot{E}^{\mathrm{c}}_{\mathrm{e}}}{\partial\Sigma_{\mathrm{e}}}(\dot{\Sigma}_{\mathrm{e}}\,\Delta t) \tag{21}$$

After some algebra, Eq. (16) can be finally written in the form:

$$\dot{\tau}^{ij} = L^{ijkl}\,\dot{\eta}_{kl} + \dot{\tau}^{ij}_{*}, \qquad L^{ijkl} = \mathscr{L}^{ijkl} - \mu M^{ij}_{\mathrm{A}}\,M^{kl}_{\mathrm{B}} \tag{22}$$

with

$$M^{ij}_{\mathrm{A}} = \mathscr{R}^{ijkl}\,N_{kl},\ M^{ij}_{\mathrm{B}} = \mathscr{R}^{ijkl}\,N^0_{kl},\ N^0_{ij} = \frac{3}{2}\frac{s_{ij}}{\Sigma_{\mathrm{e}}} \tag{23}$$

$$\dot{\tau}^{ij}_{*} = -\sqrt{\frac{G}{g}}\left\{\frac{1}{1+\xi}\,\dot{E}^{\mathrm{c}_{(t)}}_{\mathrm{e}}\,M^{ij}_{\mathrm{A}} + \dot{\Delta}^{ij}\right\} \tag{24}$$

$$\mu = \frac{\xi}{1+\xi}\frac{1}{h}\sqrt{\frac{G}{g}},\ h = M^{ij}_{\mathrm{B}}\,N_{ij},\ \xi = n\frac{\dot{E}^{\mathrm{c}_{(t)}}_{\mathrm{e}}}{\Sigma_{\mathrm{e}}}h\theta\,\Delta t \tag{25}$$

and with the N_{ij} and $\dot{\Delta}_{ij}$ for the two different cavitation modes being given by Eqs. (18) and (19). In this manner, time integration can be performed simply in an explicit-type manner, but with a stable time step Δt that is substantially improved by taking an appropriate value of θ; here we have used $\theta = 0.9$.

5. Results

As an example of the application of the damage model, we here analyze the HA evolution in a 2.25Cr–1.0Mo pressure vessel. What we are interested in is the gradual degradation of the material, presumably from the inside of the vessel outwards, with time. Thus, the problem we shall study is a typical continuous damage problem, where the damage is assumed to be independent of the axial coordinate x^1 and the circumferential coordinate x^3. This reduces the problem to an essentially one-dimensional one, along the radius x^2 or r. With these propositions, the virtual work rate condition Eq. (15) can be simplified to involve only integration over the wall thickness from initial inner radius $r_{\mathrm{i,I}}$ to outer radius $r_{\mathrm{o,I}}$ (see Fig. 1). For the latter, a finite element solution is sought by using simple one-dimensional elements with standard Gaussian integration points. The wall is discretized into 20 elements.

To make the discussion specific, the vessel is taken to have an initial internal radius of $r_{\mathrm{i,I}} = 1.62$ m and an initial outer radius of $r_{\mathrm{o,I}} = 1.78$ m. The operating conditions, which are the temperature, the absolute pressure and the partial hydrogen pressure inside the vessel, are $T_{\mathrm{i}} = 693$ K, $p = 14.3$ MPa and $p_{\mathrm{H_2,i}} = 12.8$ MPa, respectively. We assume that the pressures outside the vessel are zero, thus also $p_{\mathrm{H_2,o}} = 0$ and that the temperature at the outer surface of the vessel is $T_{\mathrm{o}} = 683$ K. We assume steady state conditions, so that the radial distribution of the temperature $T(r)$ and hydrogen pressure $p_{\mathrm{H_2}}(r)$ are given by:

$$T(r) = T_{\mathrm{o}} - (T_{\mathrm{o}} - T_{\mathrm{i}})\frac{\ln(r/r_{\mathrm{o}})}{\ln(r_{\mathrm{i}}/r_{\mathrm{o}})} \quad \text{and}$$

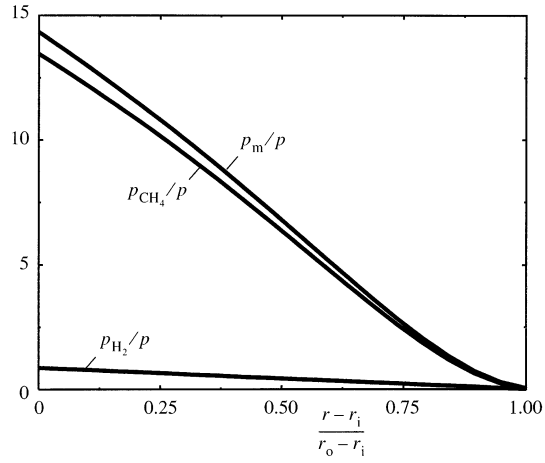

Fig. 4. Distribution of the hydrogen pressure, methane pressure and cavity pressure, normalized by the vessel internal pressure along the vessel wall for a M_3C carbide.

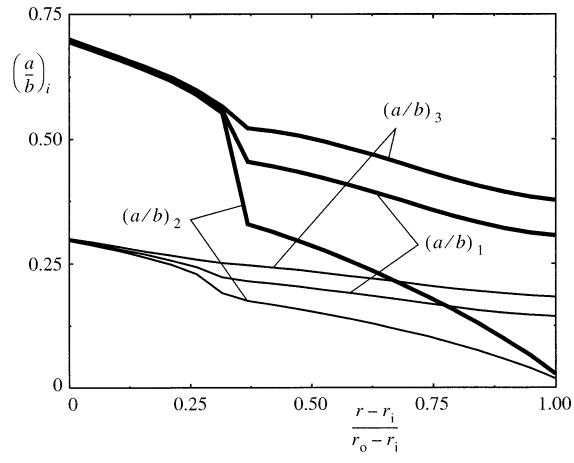

Fig. 5. Distribution of cavitation damage along the three families of facets, expressed in $(a/b)_i$, along the vessel wall at various times: thin lines, after 23 years; thick lines, at failure after 91 years.

$$p_{H_2}(r) = p_{H_2,o} - (p_{H_2,o} - p_{H_2,i}) \frac{\ln(r/r_o)}{\ln(r_i/r_o)}. \quad (26)$$

As most pressure vessels are relatively long, the axial strain-rate $\boldsymbol{D}:\boldsymbol{m}_1$ is assumed to be constant over the wall and its value is determined so that the resulting axial force in the vessel balances the axial resultant force due to the internal pressure p.

The material parameters for a 2.25Cr–1.0Mo steel are collected from literature. We note that the actual properties of a steel depend very strongly on the processing treatment, in particular the heat treatment. Moreover, accurate values of some parameters, such as the diffusion coefficient, are hard to obtain from experiments. The parameters employed in the HA analyses are the following. Young's modulus at the mean wall temperature of $(T_i + T_o)/2 = 688$ K is $E = 1.8 \times 10^5$ MPa, Poisson's ratio is $v = 0.3$ and the linear thermal expansion coefficient is $\alpha = 16.8 \times 10^{-6}$ K^{-1}. The variation of these thermoelastic properties over the vessel wall due to the temperature gradient is neglected. The creep parameters are $\dot{\varepsilon}_0 = 2.1 \times 10^{-64}$ s^{-1} when taking $\sigma_0 = 1.0$ N m^{-2} and $n = 6.5$ at $T_0 = 727$ K [26]. For the corresponding activation energy for creep we have used $Q_V = 251 \times 10^3$ J mol^{-1} from [18]. The grain boundary diffusion coefficient is taken as $\mathscr{D}_0 = 1.7 \times 10^{-35}$ m^2 s^{-1} at $T_0 = 727$ K with a corresponding activation energy $Q_B = 206 \times 10^3$ J mol^{-1} [3]. The initial average facet radius is taken as $R_I = 48$ μm, while the cavities are taken to have an average initial half spacing of $b_I = 4$ μm and an initial radius of $a_I = 0.04$ μm.

The methane pressure inside the cavities depends strongly on the cavity stability and varies with the local temperature and hydrogen pressure (see e.g. [6]). We here assume the rather aggressive carbide, M_3C consisting of 30% Cr, which will result in a conservative lifetime prediction. The methane pressure is calculated with a standard equilibrium reaction model of the hydrogen-methane reaction described in [6], which builds on the work of (among others) Lundberg et al. [27], Odette and Vagarali [28] and Parthasarathy and Shewmon [29]. The influence of Mo on the methane pressure is neglected since thermodynamic data are not available for Mo. The cavity pressure distribution along the radius of the vessel wall under the operating conditions described above is plotted in Fig. 4. It is seen that the highest methane pressure is at the inner radius and decreases with decreasing hydrogen pressure.

The distribution of cavitation damage, expressed by the value of the damage parameters $(a/b)_i$ over each of the three families of facets ($i = 1, 2, 3$), along the vessel radius after 23 years of operation is plotted in Fig. 5. The cavitation damage in the circumferential direction, $(a/b)_3$,

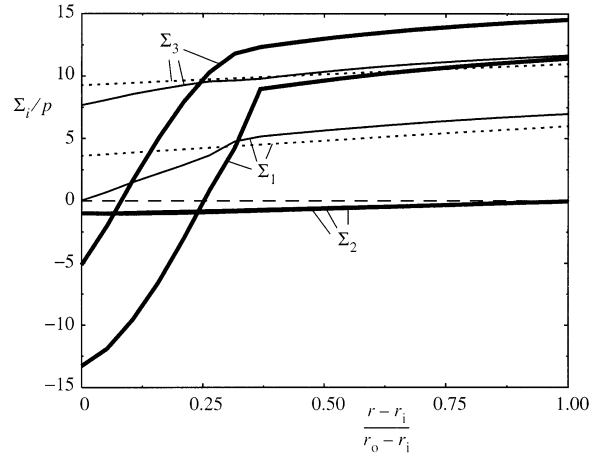

Fig. 6. Stress distribution along the wall at various times: dotted lines, pure creep solution (no grain boundary cavitation); thin lines, after 23 years; thick lines, at failure. The stresses are normalized by the vessel pressure p.

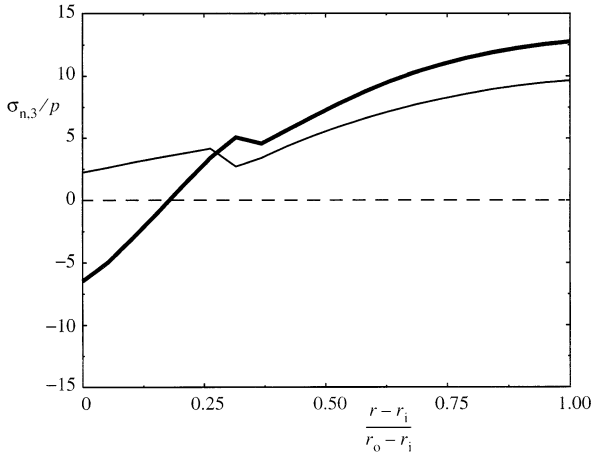

Fig. 7. Distribution of $\sigma_{n,3}$ along the vessel wall: thin lines, after 23 years; thick lines, at failure after 91 years.

is largest, followed by the cavitation $(a/b)_1$ in axial direction. The cavitation in the radial direction is only significant wherever the rigid grain mode is active. The two cavitation modes cannot be clearly distinguished from the plot in Fig. 5, but it was found that to the inner side, for $(r-r_i)/(r_o-r_i)<0.3$), the rigid grain mode is active, whereas the penny shaped crack mode is active at the outer side. In the beginning of the process, the penny shaped crack mode was active throughout the wall thickness. Then, starting at the inner radius, the rigid grain mode takes over, reaching a stable location at the above mentioned position. Failure occurs after 91 years by coalescence on facets perpendicular to the circumferential direction, $(a/b)_3=0.7$. The cavitation distribution is displayed in Fig. 5. The transition between the cavitation modes can now be seen more distinctly. The damage distributions are not smooth anymore since a gradual transition between both cavitation modes is not accounted for in the damage model [11].

The corresponding distributions of the macroscopic principal stress components Σ_i are shown in Fig. 6. In order to obtain good insight in the influence of the HA cavitation, the stress distribution in the absence of any grain boundary cavitation is shown for reference. This is plotted in Fig. 6 after just 6 years, thus representing the situation at steady state creep when finite strains, which would develop after long time, are still negligible. In that case, for the chosen geometry, all stress components vary only slowly over the wall thickness, with the minimum values at the inner radius. The circumferential stresses Σ_3 are twice the axial stresses. The radial stress Σ_2 increases nearly linearly from $\Sigma_2/p=-1$ to zero at $r=r_o$.

In the same figure, Fig. 6, the stress distribution is plotted for the pressure vessel with HA after 23 years when $(a/b)_3=0.3$ at the inner radius. Due to the rapid dilation of the material by cavitation in the rigid grain mode at the inner radius, the axial and circumferential stresses, Σ_1 and Σ_3 respectively, have relaxed. The stresses are reduced sufficiently to maintain compatibility in strain. By virtue of overall equilibrium with the vessel pressure p, Σ_1 and Σ_3 near the outer radius have therefore increased somewhat. The kink in the slope of the distributions are again close to the position of transition between cavitation modes. In the stress distributions just prior to failure, the mentioned effects are even more pronounced. At the inner radius, the dilational strain-rate due to HA cavitation is so fast that this has to be constrained by compressive stresses in order to maintain compatibility; as a consequence, the stresses near the outer radius reach a higher level. The distribution of radial stress, Σ_2, seems to be hardly affected by the HA cavitation.

Fig. 7 shows the distribution of the normal stress $\sigma_{n,3}$ acting on the facet perpendicular to the circumferential direction. The distribution after 23 years shows that the normal stress is tensile, so as to accelerate the grain boundary cavitation. The kink is due to change between the cavitation modes. Just prior to failure, after 91 years, the normal stresses are compressive over part of the vessel wall, thus decelerating the cavitation rate. At the outer side, the normal stress distribution is still tensile, and increased in magnitude, just like the macroscopic circumferential stress Σ_3.

For the case discussed so far, the cavities grow primarily by diffusion. The minimum value of the ratio $\dot{V}_{diff}/\dot{V}_{cr}$ is observed at the inner radius, with $\dot{V}_{diff}/\dot{V}_{cr}=12$ prior to coalescence at $(a/b)_3=0.7$. At $(a/b)_3=0.3$, we find $\dot{V}_{diff}/\dot{V}_{cr}=480$.

The creep rate enhancement due to grain boundary cavitation is expressed in $g_c=(\boldsymbol{D}^{CC}:\boldsymbol{m}_3)/(\boldsymbol{D}^{C}:\boldsymbol{m}_3)$, where $\boldsymbol{D}^{C}$ is defined in Eq. (8). The maximum of g_c observed at $(a/b)_3=0.30$ is 2.44 at the inner radius, whereas $g_c=1.10$ at the outer radius. Prior to failure, $g_c=10.4$ at the inner radius and is as low as 1.07 at the outer radius. This means that the cavitation at the outer radius hardly affects the creep rate, so that the presence of cavitation there plays a minor role. The circumferential logarithmic strains at failure are $E_{3,i}=\ln(r_i/r_{i,I})=0.009$ and $E_{3,o}=\ln(r_o-r_{o,I})=0.008$ and the axial strain is $E_1=0.003$.

To gain some feeling about which material parameters are most important, we now investigate some parameter variations. We first increase the reference creep strain-rate by a factor 10, so that $\dot{\varepsilon}_0=2.1\times10^{-63}\,s^{-1}$. Then, the rigid grain mode is not activated during lifetime; the penny shaped crack mode of cavitation completely dominates. The time to failure is now decreased to 62 years. Coalescence occurs again on facets perpendicular to the circumferential direction, and close to the inner radius. The normal stresses $\sigma_{n,3}$ are tensile during most of the lifetime, but become compressive at the inner radius when $(a/b)_3=0.6$. The macroscopic stresses Σ_i are then

still tensile. Though diffusive growth is still important, the minimum ratio is $\dot{V}_{\text{diff}}/\dot{V}_{\text{cr}} = 3.8$ prior to failure at a quarter of the wall. The creep enhancement by cavitation at $(a/b)_3 = 0.3$ at the inner radius is $g_c = 1.10$ and at the outer radius $g_c = 1.01$. Just prior to failure, g_c has increased $g_c = 4.65$ at the inner radius and $g_c = 1.01$ at the outer radius. The circumferential strains at failure are now substantially larger than before: $E_{3,i} = 0.031$, $E_{3,o} = 0.026$ whereas the axial strain is negligible.

When, instead, the reference strain-rate is decreased to $\dot{\varepsilon}_0 = 2.1 \times 10^{-65}\ \text{s}^{-1}$, cavitation damage proceeds according to the rigid grain mode nearly during the entire lifetime. The lifetime of the vessel is now 113 years. The stresses Σ_1 and Σ_3 near the inner radius become highly compressive, comparable to those shown in Fig. 6. So, again, the normal stresses are constraining the HA evolution.

Increasing the grain boundary diffusion parameter by a factor 10 to $\mathscr{D}_0 = 1.7 \times 10^{-34}\ \text{m}^2\,\text{s}^{-1}$ reduces the lifetime to 11.3 years. As expected, the rigid grain mode is dominant during most of the lifetime, although the penny shaped crack mode takes over near the end of the lifetime at the outer side, due to relatively high stresses Σ_1 and Σ_3. Decreasing the diffusion parameter by a factor 10, down to $\mathscr{D}_0 = 1.7 \times 10^{-36}\ \text{m}^2\,\text{s}^{-1}$, results in a predicted lifetime of 620 years. As expected, only the penny shaped crack mode is active in this case since the diffusive contribution to cavity growth is now an order of magnitude smaller.

Also the parameters concerning the cavities and carbides have been varied. Increasing the initial cavity radius by a factor of 10 barely influences the results, as is well-known in literature (see e.g. [2]). However, halving the initial half spacing to $b_I = 2$ μm (i.e. four times more carbides) changes the evolution drastically. The time to first cavity coalescence is now 12 years. The location of the transition between cavitation modes is at three-quarters of the vessel wall. The opposite effect occurs when taking $b_I = 6$ μm. The lifetime is then 290 years and the rigid grain mode of cavitation plays a minor role. Only near the inner radius a small and slowly increasing area emerges where the rigid grain mode is active. Another important parameter is the stability of the carbides. The stability of the carbides is determined by the tempering temperature and tempering time of the steel [30]. The longer the time and the higher the temperature, the more aggressive carbides like M_3C change into more stable carbides like M_7C_3. Assuming, instead of the aggressive M_3C carbide, the more stable M_7C_3 carbide with 60% Cr content we find a lifetime of 232 years instead of 91 years. Again, the rigid grain mode is active only near the end of the lifetime and only then does the axial stress become compressive at the inner radius to constrain cavitation. The maximum cavity pressure found in the wall, $p_m/p = 3.96$, is much lower than the axial and circumferential stresses, especially in the beginning of the process. Therefore, it appears that failure in this case may be better classified as intergranular creep cavitation assisted by HA rather than as a 'pure' HA failure mode due to relatively high methane pressures.

As another variation of the parameters in the model that characterize the operating conditions, we consider a case in which the internal pressure is increased to $p = 19.0$ MPa and the partial hydrogen pressure to $p_{H_2,i} = 17.2$ MPa. The maximum cavity pressure now increases to $p_m/p = 14.3$ (note that also p has increased). Due to the higher loading of the vessel wall, the rigid grain mode is only active after $(a/b)_3 = 0.6$ near the inner wall. The lifetime reduces to 59 years, while the strain at failure is substantially larger: $E_{3,i} = 0.021$, $E_{3,o} = 0.017$ and $E_1 = 0.001$. The creep acceleration due to cavitation found near the inner radius is $g_c = 2.92$, while $g_c = 1.03$ at the outer radius just prior to failure.

Increasing the operating temperature T_i by 30 K and assuming that the outer temperature then also increases by 30 K, has a more dramatic effect. The new lifetime estimate is 29 years though the maximum cavity pressure is reduced to $p_m/p = 9.79$. This indicates that the decrease of cavity pressure with increasing temperature cannot compensate for the increase in creep and diffusion rates. Decreasing the outer temperature by 10 K to $T_o = 673$ K, on the other hand, increases the lifetime to 101 years. This is due to the fact that the creep resistance near the outer wall of the vessel is increased so that the development of cavitation damage near the inner wall is further constrained.

Changing the geometry of the vessel slightly by assuming the inner radius to be $r_{i,I} = 1.64$ m, results in an increased stress level in the wall. The overall development of HA however does not change much qualitatively, except that the rigid grain mode of cavitation is somewhat less active, and the lifetime reduces to 83 years. Reducing the outer radius to $r_{o,I} = 1.76$ m results in a predicted lifetime of 84 years.

The predicted times to failure due to HA, as discussed sofar, may depend on the model assumptions used. For instance, one may argue that the rigid grain mode is a strong simplification of the real behaviour: uniform cavitation of all facets in a polycrystalline RVE may be debatable. To check the effect of this assumption, we repeat the central case shown in Figs. 5–7, but with the possibility of the rigid grain mode removed from the constitutive equations, so that cavitation only takes place according to the penny shaped crack mode. Moreover, to make interaction between facets unlikely, we reduce the value of ρ from 1.04 to 0.5. The predicted lifetime with the penny shaped crack model is now 219 years instead of 91 years previously. Though most HA distributions discussed in the foregoing exhibited a more or less similar distribution over the wall thickness with most cavitation at the inner radius (c.f. Fig. 5), the distribution found without the rigid grain mode is quite different: first

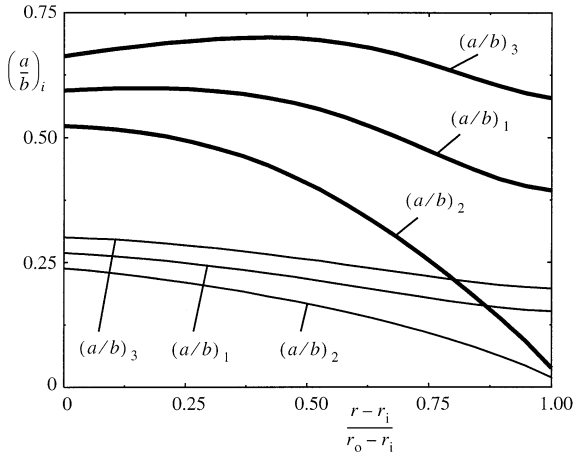

Fig. 8. Distribution of cavitation damage, expressed in $(a/b)_i$, along the vessel wall in case of the constitutive relations without rigid grain mode cavitation: thin lines, after 28 years; thick lines, at failure after 219 years.

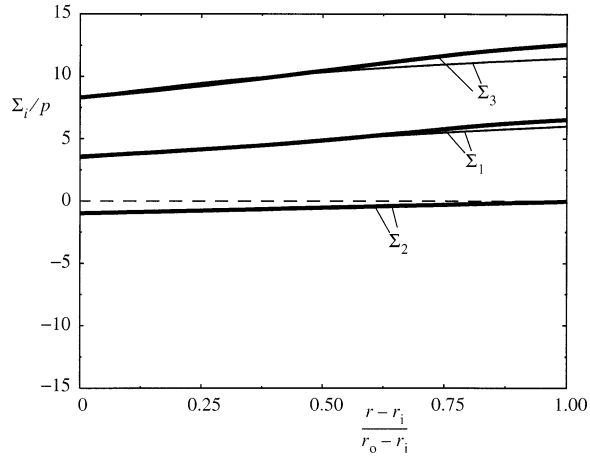

Fig. 10. Macroscopic stress distribution after 28 years (thin lines) and after 219 years (thick lines).

cavity coalescence occurs in the middle of the wall, as can be seen in Fig. 8. In the beginning, the maximum cavitation is at the inner radius of the wall (see, e.g. the distribution after 28 years) and during evolution the maximum slowly moves outwards. The facet normal stress distribution in the circumferential direction, $\sigma_{n,3}$, is plotted in Fig. 9 together with the internal cavity pressure p_m. One can see that the difference between the methane pressure distribution and this facet stress becomes relatively small in the course of the process. This shows that cavitation is strongly creep constrained, which agrees with the fact that diffusion is found to be the dominant cavity growth mechanism. An important thing to notice from Fig. 8 is that, over the inner half of the vessel, the cavitation damage developing on the three families of facets is roughly the same. Even in the absence of therigid grain cavitation mode, the amounts of damage in the principal directions are comparable. This demonstrates that it is indeed important to incorporate the cavitation in all three directions, rather than only in the direction of the maximum applied principal stress as was done in [13]. This is partly due to the macroscopic stress distribution, shown in Fig. 10; but, the reason for cavitation in the radial direction can only be explained from the cavity gas pressure p_m. Nevertheless, the lifetime prediction for this vessel is not changed by the extension relative to [13], since the maximum principal stress direction remains in the circumferential direction throughout the lifetime.

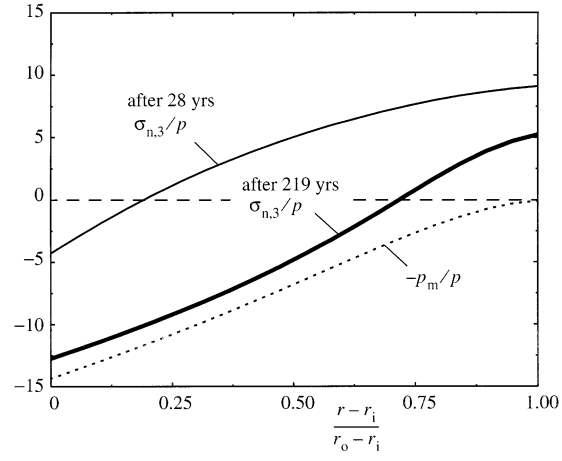

Fig. 9. Distribution of the cavity pressure p_m (dashed line) and of the normal stress $\sigma_{n,3}$ (solid line): thin lines, after 28 years; thick lines, at failure after 219 years.

The lifetime prediction using only the penny shaped crack mode depends sensitively on the creep parameters used. Increasing the reference creep strain-rate to $\dot{\varepsilon}_0 = 2.1 \times 10^{-63}\ s^{-1}$, as done earlier in the above, reduces the predicted lifetime by a factor of almost down to 57 years. Taking the more stable carbide M_7C_3 used above gives a lifetime prediction of 286 years, with cavity coalescence taking place at the inner radius. Without the rigid grain mode, the creep rate enhancement g_c is lower. This is only partly due to the lower value of ρ in Eq. (11), since the lifetime depends relatively weakly on ρ as a consequence of the internal stress redistributions associated with constrained damage evolution. Taking $\rho = 0.2$ instead of 0.5, for example, gives a lifetime prediction of 197 years. The fact that this is even slightly smaller than the value for $\rho = 0.5$ is due to subtle differences in the stress redistributions. Due to the fact that the number of cavitating grain boundary facets contributing to the creep-cavitation strain-rate is smaller for $\rho = 0.2$, the reduction of the stress level near the inner radius for the present material parameters is slower than for $\rho = 0.5$, which eventually leads to a slightly faster damage process.

6. Discussion

In this paper, we analyzed hydrogen attack (HA) in a 2.25Cr–1Mo pressure vessel by means of a damage model. This damage model gives the macroscopic strain-rate and cavitation rate of a polycrystalline representative volume element as function of the temperature, hydrogen pressure and applied stresses. Thus, the temperature dependence of the cavity growth mechanisms, diffusion and creep, and the dependence of the methane pressure on carbide stability, temperature and hydrogen pressure are incorporated. The interaction of the grain boundary cavitation with the adjacent grains is modeled for the two extreme cavitation modes; the one yielding the largest cavitation rate is the active one. In the one extreme, where cavitation is virtually uniform along facets, it is modeled by the rigid grain model. In the other extreme, where creep deformations of the grain are significant, so that cavitation takes place primarily on facets perpendicular to the maximum principal macroscopic stress, the cavitation is modeled with an extended penny shaped crack model. The extension involves accounting for cavitation in all three principal directions.

The predictions with the model presented here are only intended to give an indication of trends and sensitivity to parameters. The material data used on input is gathered from various sources and is not sufficiently reliable to make real lifetime predictions.

In the analysis of the pressure vessel, it was found that HA cavitation is accelerated by the hoop stresses in the beginning of the lifetime. However, when the strain-rates due to the cavitation become sufficiently high—especially at the inner radius of the wall where the cavity pressures are very high—internal re-distribution of the stresses take place such that the cavitation is decelerated by compressive stresses. When cavitation proceeds according to the penny shaped crack mode, the grains adjacent to the facet generate the compressive stresses. Then, the polycrystal strain-rates remain relatively low and the stresses acting on the polycrystal remain tensile. When cavitation proceeds according to the rigid grain model, the strain-rates are so large that the macroscopic tensile stresses in the vessel wall change into compression in order to constrain cavitation. This was often observed close to the end of the lifetime. This means that the outer part of the wall has to constrain the dilation due to HA at the inner radius.

The jumps in porosity in Figs. 5 and 7 are due to the somewhat arbitrary criterion Eq. (13) to determine which cavitation mode is active. Both cavitation modes are extreme cavitation rate distributions, so the transition here from one extreme mode to the other is somewhat abrupt. Considering a more continuous transition between the two cavitation modes would probably eliminate most of the jump in these curves.

Cavitation in the pressure vessel appeared to not only take place on facets perpendicular to the macroscopic principal stress direction but also on other facets, even in the penny shaped crack model. This is partly due to presence of the biaxial stress state (hoop stresses) and the relatively high methane gas cavity pressure (carbides are distributed uniformly along all facets).

The parameter study demonstrated that some material parameters have a greater influence on the lifetime than others. One of the most important parameters is the density of grain boundary carbides and their stability. But the predicted lifetimes are also very sensitive to the values of the diffusion and creep parameters, as well as their temperature dependence.

This study also demonstrated how the HA susceptibility of a component can be influenced at several stages of its lifetime. At the design stage, the allowed stress level inside the wall determines the steady state creep properties. In this, also the amount of insulation fitted on the vessel wall is of importance, since it determines the temperature at the outside of the wall. During the manufacturing of the material, the heat treatment is of great importance in determining the carbide density and stability. Reducing the density of grain boundary carbides or changing them into more stable carbides will improve the vessel lifetime. Obviously the actual operation affects the HA susceptibility through the operating temperature and (hydrogen) pressure inside the vessel. Finally, maintenance of the plant has a difficult task in case of welding of the component. Most weldments result in residual stresses and unstable carbides, so that the post-weld heat treatment is important in ensuring that the most aggressive carbides be converted into more stable ones and that residual stresses are decreased.

Models describing only the evolution of one representative cavity by a cavity growth relation, e.g. [2,3,6], can only predict conservative lifetimes. This is due to the assumption that the stress state is constant during the lifetime, which has been shown here to be not valid in general. The development of tensile or compressive stresses, which tend to influence the rate of the HA process and thereby increase the lifetime, cannot be described by the single cavity models.

Also, the general applicability of the Nelson curve is questionable. The Nelson curve gives the maximum temperature and hydrogen pressure for several commonly used steels, based on industrial experiences. Due to its simplicity it is commonly used, but this simplicity is at the same time also its weakness. We demonstrated in this paper that the lifetime of a component depends sensitively on more aspects than included in the Nelson curve, such as the carbide stability or the applied stress level. This implies that the HA susceptibility of all components of the same nominal steel are not equal due to different heat treatments or different maximum stress levels. The operating limits set by the Nelson curve will be too optimistic for steels with aggressive carbides or high stress levels and too conservative for components with a proper heat treatment and low stress levels.

Acknowledgements

The research of Marc van der Burg is sponsored by Shell Research and Technology Centre, Amsterdam.

References

[1] American Petroleum Institute Publication 941, 4th edn., 1990.
[2] H.M. Shih, H.H. Johnson, Acta Metall. 30 (1982) 537.
[3] T.A. Parthasarathy, Acta Metall. 33 (1985) 1673.
[4] P.G. Shewmon, Acta Metall. 35 (1987) 1317.
[5] E. van der Giessen, M.W.D. van der Burg, A. Needleman, V. Tvergaard, J. Mech. Phys. Solids 43 (1995) 123.
[6] M.W.D. van der Burg, E. van der Giessen, R.C. Brouwer, Acta Mater. 44 (1996) 505.
[7] M.W.D. van der Burg, E. van der Giessen, Mater. Sci. Eng. A220 (1996) 200.
[8] B.F. Dyson, Metal Sci. 10 (1976) 349.
[9] V. Tvergaard, J. Mech. Phys. Solids 32 (1984) 373.
[10] E. van der Giessen, V. Tvergaard, Acta Metall. Mater. 42 (1994) 959.
[11] M.W.D. van der Burg, E. van der Giessen, Acta Mater. 45 (1997) 3047.
[12] V. Tvergaard, Acta Metall. 32 (1984) 1977.
[13] M.W.D. van der Burg, E. van der Giessen, V. Tvergaard, in: H. Nisitani, et al. (Eds.), Localized Damage IV: Computer-Aided Assessment and Control, Computational Mechanics, Southampton, 1996, p. 641.
[14] D. Hull, D.E. Rimmer, Phil. Mag. 4 (1959) 673.
[15] A. Needleman, J.R. Rice, Acta Metall. 28 (1980) 1315.
[16] T.L. Sham, A. Needleman, Acta Metall. 31 (1983) 919.
[17] B. Budiansky, J.W. Hutchinson, S. Slutsky, in: H.G. Hopkins, M.J. Sewell (Eds.), Mechanics of Solids: The Rodney Hill 60th Anniversary Volume, Pergamon Press, Oxford, 1982, p. 13.
[18] H.J. Frost, M.F. Ashby, Deformation-Mechanism Maps, Pergamon Press, Oxford, 1982, p. 62.
[19] P.G. Shewmon, Mater. Sci. Technol. 1 (1985) 1.
[20] A.C.F. Cocks, M.F. Ashby, Prog. Mater. Sci. 27 (1982) 189.
[21] J.R. Rice, Acta Metall. 29 (1981) 675.
[22] M.Y. He, J.W. Hutchinson, J. Appl. Mech. 48 (1981) 830.
[23] J.W. Hutchinson, Acta Metall. 31 (1983) 1079.
[24] E.T. Onat, F.A. Leckie, J. Appl. Mech. 55 (1988) 1.
[25] S. Murakami, J. Appl. Mech. 55 (1988) 280.
[26] H.E. Boyer, Atlas of Creep and Stress-Rupture Curves, ASM International, Ohio, 1988, pp. 1926–1946.
[27] R. Lundberg, M. Waldenström, B. Uhrenius, CALPHAD 1 (1977) 159.
[28] G.R. Odette, S.S. Vagarali, Metall. Trans. 13A (1982) 299.
[29] T.A. Parthasarathy, P.G. Shewmon, Metall. Trans. 15A (1984) 2021.
[30] R.G. Baker, T. Nutting, J. Iron Steel Inst. (1959) 257.